Original Article
pISSN 2383-5389 / eISSN 2383-8116
Journal of International Society for Simulation Surgery 2015;2(1):17-25
http://dx.doi.org/10.18204/JISSiS.2015.2.1.017

Unscented Kalman Snake for 3D Vessel Tracking

Sang-Hoon Lee, Sanghoon Lee

Department of Electrical and Electronic Engineering, College of Engineering, Yonsei University, Seoul, Korea

Purpose In this paper, we propose a robust 3D vessel tracking algorithm by utilizing an active contour model and unscented Kalman filter which are the two representative algorithms on segmentation and tracking.

Materials and Methods The proposed algorithm firstly accepts user input to produce an initial estimate of vessel boundary segmentation. On each Computed Tomography Angiography (CTA) slice, the active contour is applied to segment the vessel boundary. After that, the estimation process of the unscented Kalman filter is applied to track the vessel boundary of the current slice to estimate the inter-slice vessel position translation and shape deformation. Finally both active contour and unscented Kalman filter are inter-operated for vessel segmentation of the next slice.

Results The arbitrarily shaped blood vessel boundary on each slice is segmented by using the active contour model, and the Kalman filter is employed to track the translation and shape deformation between CTA slices. The proposed algorithm is applied to the 3D visualization of chest CTA images using graphics hardware.

Conclusion Through this algorithm, more opportunities, giving quick and brief diagnosis, could be provided for the radiologist before detailed diagnosis using 2D CTA slices, Also, for the surgeon, the algorithm could be used for surgical planning, simulation, navigation and rehearsal, and is expected to be applied to highly valuable applications for more accurate 3D vessel tracking and rendering.

Key Words Vessel Tracking · Active Contour · Snake · Unscented Kalman Filter.

Received: May 12, 2015 / **Revised:** May 15, 2015 / **Accepted:** May 28, 2015
Address for correspondence: Sanghoon Lee
The department of Electrical and Electronic Engineering, Yonsei University, 50 Yonsei-ro, Seodaemun-gu, Seoul 120-749, Korea
Tel: 82-2-2123-2767, **Fax:** 82-2-313-2879, **E-mail:** slee@yonsei.ac.kr

Introduction

Via the rapid development of current image processing technologies based on image segmentation, tissue characterization and image registration, various medical technology fields, such as diagnosis decision and therapy planning, are working toward a common platform of medical image processing. Even the area of vessel tracking is following this trend. As a result, vessel tracking methods for different human organs have been proposed by developing application oriented image processing algorithms based on a common platform. However, the size of data needing to be manipulated is growing remarkably due to advances in image acquisition technology, as well as clinical requirements. In addition, the expectations for diagnostic accuracy are higher in line with the larger number of applications utilizing image processing. For this reason, it is necessary to develop image processing algorithms to achieve such basic requirements in terms of robustness, precision, and reproducibility. Moreover, to apply developed algorithms in the field, it is important to have an accessible user interface and timing synchronization performance in parallel with performance accuracy (1).

In conventional research, there are two types of vessel segmentations: the *model-based* approach (2-4) and the *tracking-based* approach (5, 6). In the model-based approach, segmentation is achieved by using content information such as the pattern and shape of the target objects. This approach is very effective to track an object even if it has a slight deformation or variation in translation, rotation, or magnification, as opposed to a radical structural deformation. For the model-based approach, the most representative approach is an active contour algorithm (7). The algorithm, also called *snake*, creates its contour from the initial contour created by user input to the target object by deforming the shape of the contour. This algorithm has demonstrated good performance in 2D object segmentation, but proper segmentation in a 3D environment is not com-

mon. Furthermore, it is difficult to apply this algorithm directly to the tracking of drastic shape changes in a vessel boundary.

On the other hand, the tracking-based approach segments and tracks each vessel by applying a local operator around the vessel. At the first Computed Tomography/Magnetic Resonance Imaging (CT/MRI) slice, it detects the centerline or boundary of the vessel. This tracking is then performed consecutively for the following slices based on the initial detection at the first slice. This method makes it possible to reduce user intervention and consequently leads to a considerable decrease in computation cost after the initial segmentation. In the tracking-based approach, the most commonly used method is the Kalman filter algorithm. This algorithm consists of a series of tracking states defined by using a linear state-space model. It is also available to track the structure of a vessel in a 3D environment because the state-space model can be applied to track the shape variation of the vessel boundary between slices. However, it is easy to fail to segment the vessel because of the ambiguous boundary of vessels when they are adjacent to the bone, which in turn leads to a failure to trace the vessel for the subsequent slices due to the propagation of such improper segmentation. Moreover, since the shape variation between slices has a non-linear characteristic, the Kalman filter hardly obtains a proper result due to its linear state-space model. To overcome this problem, various extensions of the Kalman filter have been devised to track such nonlinear systems - extended and unscented Kalman and particle filters (8-12). In an unscented Kalman (UKF), the problem is resolved using the nonlinear model directly without linearizing it with specific points selected through the probabilistic distribution of estimated values (11).

In this paper, we present a scheme named the unscented Kalman snake for vessel tracking by taking advantage of both model-based and tracking based approaches, which allows a resilience for shape deformation and a reduction in user intervention. Based on these two approaches, we sought to develop a unique algorithm incorporating the active contours and unscented Kalman filter schemes. First, we employ an active contour model for initializing the vessel boundary. The estimation process of the unscented Kalman filter is then applied to track the vessel boundary of the first slice to estimate the inter-slice vessel position translation and the shape deformation. Finally, both processes are inter-operated so as to perform vessel segmentation for the next slice.

The layout of the paper is as follows: Section II provides materials and methods, and results are given in section III. Discussion and conclusions are presented in sections IV and V respectively.

Materials and Methods

Motivation

In this paper, we present a vessel tracking algorithm by utilizing snake for finding the contour of a vessel in each intra slice and the unscented Kalman filter for finding the 3D blood ves-

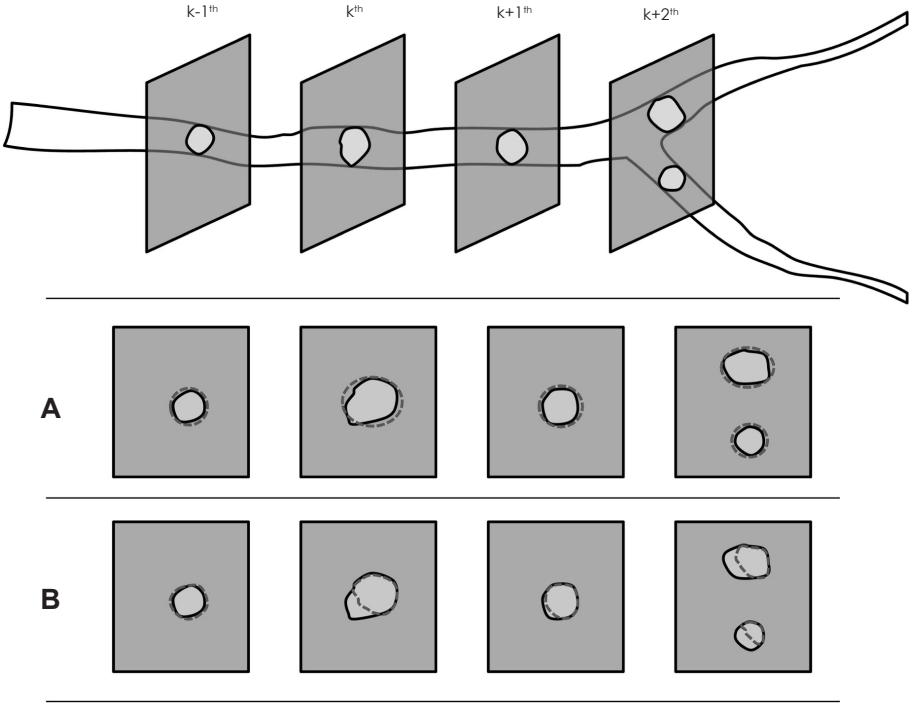

Fig. 1. Outline of the vessel tracking system: the solid line is the vessel boundary and the dotted line is the estimated boundary. A: Classical Kalman filter only. B: Active contour model only.

sel among the inter slices, and attempt to take advantage of combining the two algorithms to overcome the drawbacks of each method.

Generally, the attributes of the contour include the centroid and the major and minor axes of an ellipse. However, if the unscented Kalman filter is used alone, it is difficult to accurately track an irregular shape variation of the boundary. Fig. 1A shows that the boundary obtained by the unscented Kalman filter (dotted line) is not tightly matched with the vessel boundary.

Moreover, the snake has the ability to segment the irregular shape of a boundary more accurately than the unscented Kalman filter. However, if the snake is solely applied to tracking, the contour cannot evolve because the algorithm does not consider the shape variation between two consecutive slices. In other words, without any information of the inter-slice shape variation, the algorithm has no choice but to track the current slice from the detected positions of the previous slice. Thus, if the shape of the boundary changes rapidly, it is difficult to segment the boundary of the current slice, despite successful segmentation in the previous slice. This situation is described well in Fig. 1B, where the dotted line for the snake does not tightly follow the vessel boundary. The k^{th} slice in Fig. 1B illustrates that the upper right part of the contour is adequately segmented in conjunction with the boundary of vessel, but the lower left part of the contour is not. The reason for the improper segmentation of the lower left part arises from the distance between the starting position of the snake and the vessel boundary. In case of the upper right image, the initial position is close to the boundary for the snake iteration, but the lower left is quite far from the boundary, resulting in a condensation of the curve due to the internal elastic force of the snake.

For realization of snake, the intrinsic parameters including the tension and rigidity of contour, pixel intensity, edge intensity, etc. can be used to track the shape deformation between CTA slices of the blood vessel. Similarly, to track the nonlinear variation of its shape deformation and the global motion of the vessel boundary between slices, the unscented Kalman filter is employed for stable result of the algorithm. In addition, the vessel contour obtained by using snake is re-sampled as the discrete version, which is then used as the state and measurement vector for the tracking system. This sampling process makes it possible to reduce the dimension of the state vector, which leads to a decrease in the computational cost.

Fig. 2 shows the schematic diagram of the proposed vessel tracking algorithm composed of the initialization and iteration processes. The initialization is conducted by using a series of processes: (a) For the first slice, L points input through the user interface are entered to construct a point set and are constrained

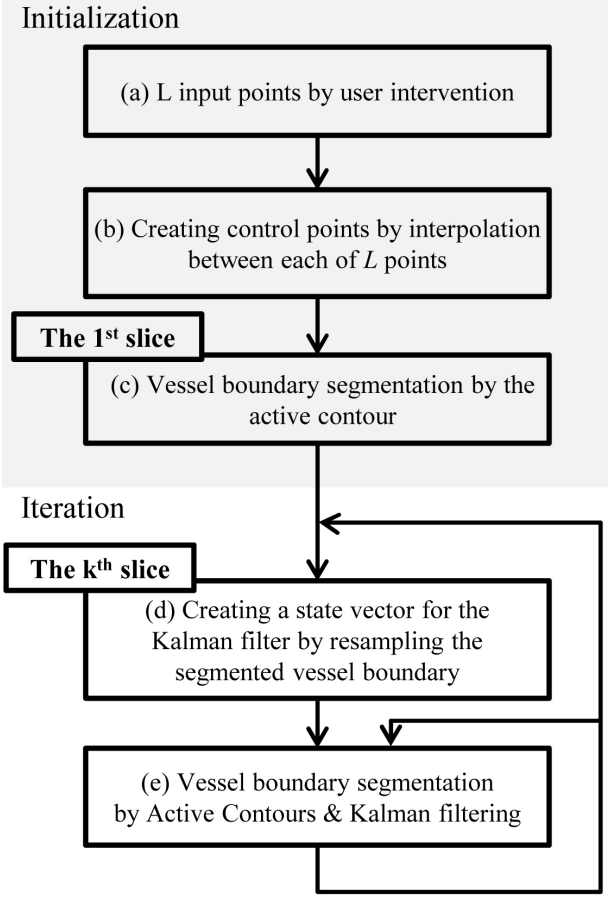

Fig. 2. Schematic diagram of the unscented Kalman snake for 3D vessel tracking.

to be located around the vessel boundary; (b) The points are interpolated to produce the initial control point set; (c) The first vessel boundary estimated by using the point set is obtained by using snake for the first slice. When the initialization process for the first slice is complete, the iteration process, which is a main process of the tracking procedure, is continued; (d) It then generates a state vector for the unscented Kalman filter by resampling the control points at the vessel boundary obtained from the k-1^{th} slice. This state vector is used as an initial vector for the k^{th} slice as an input vector for the procedure of (e); (e) Finally, the algorithm segments the vessel boundary for the k^{th} slice by applying snake and the unscented Kalman filter and then obtains control points at the vessel boundary of the k-1^{th} slice.

Backgrounds

Active Contour, Snake

The active contour model (7), (13), also known as snake, has been widely used for finding the boundary of an object in the field of computer visioning or image processing. The snake

scheme firstly accepts a user input, called *control points*, which can be used as the initial points of the snake iteration. Then the initial points are interpolated to form an initial contour. Through snake algorithm, the initial contour around the object moves elastically toward the boundary of the target object, while shrinking its shape fitting to the shape of the target object by minimizing its own energy function. Conceptually, the energy function defined in Snake has an analogous meaning to the energy used in the laws of physics so that snake transforms its shape by controlling the energy function, and the prefix 'active' indicates that the contour evolves its shape toward minimizing its energy. Relying on the definition of the energy function, Snake can have variable characteristics, including smoothness and circularity.

The energy function E_{snake} can be formulated as a summation of two energy terms, internal energy (E_{int}) for the intrinsic property of the curve itself and external energy (E_{ext}) for the image difference between the curve and the background image:

$$E_{\text{snake}}=E_{\text{int}}+E_{\text{ext}} \tag{1}$$

For example, the intrinsic property is like the length or curvature of the curve, and the image difference represents the structural difference between the curve and the background image, such as edge or additional constraints added by an external user.

Internal Energy and Force

The internal energy of snake corresponds to the intrinsic energy of the curve itself. For realization of snakes, an arbitrary curve is utilized to determine the contour of the vessel by changing the shape of the curve fitting into that of the contour of the vessel. If we want to make the curve more elastic, like a rubber band, an additional term can simply be added to show that the internal energy also relies on the length of the curve. In addition, if we want to control the smoothness of the shape, another energy term should be added to the internal energy.

Mathematically, the elasticity (the former) and the smoothness (the latter) can be controlled by utilizing the magnitudes of the first-order and second-order derivatives, respectively. Let $v(s)=((x(s), y(s)), 0\leq s\leq 1$, be the curve to be designed. The internal energy of snake then becomes

$$E_{\text{int}}=\int_0^1 \frac{\alpha(s)}{2}|\mathbf{v}_s(s)|^2+\frac{\beta(s)}{2}|\mathbf{v}_{ss}(s)|^2\,ds \tag{2}$$

where $\alpha(s)$ and $\beta(s)$ are control parameters regarding the contribution of each variable obtained from the first- and second-order derivatives to the internal energy. Greater $\alpha(s)$ influences on the elasticity of the contour between consecutive iterations, representing an effect of increasing or decreasing its circumference. Similarly, a higher $\beta(s)$ forces the contour to have a smoother shape. Numerically, the continuous integral of (2) can be approximated to the discrete sum utilizing L control points as:

$$E_{\text{int}}=\sum_{i=1}^{L}\frac{\alpha_i}{2}|\mathbf{v}_i-\mathbf{v}_{i-1}|^2+\frac{\beta_i}{2}|\mathbf{v}_{i-1}-2\mathbf{v}_i+\mathbf{v}_{i+1}|^2 \tag{3}$$

where v_0-v_L .

In snake, the contour is forced to deform its shape and size toward the direction of force to minimize the energy in (3) at each iteration. Based on the laws of physics, the direction and magnitude of force applied at each iteration can be obtained by differentiating the energy function by the displacement term of v_i-v_{i-1}.

External Energy and Force

In the snake energy function, there is another energy termed external energy, which indicates the energy between snake and the background image. If we want to extend the contour into the brighter boundary of an object, the external energy function needs to be designed based on the image's gray values $I(x_i, y_i)$ on the control point (x_i, y_i). If we hang snake on the bright boundary pixels of an object in the background image, the external energy function should be designed based on the image's gray values $I(x_i, y_i)$ on the control point (x_i, y_i). Moreover, to fit the contour to the edge of the image, an energy term regarding the image gradient $\nabla I(x_i, y_i)$ needs to be added. Based on the two aforementioned energy terms, the external energy of the contour including the two energy terms becomes:

$$E_{ext}=-\sum_{i=1}^{L}\left(w_{line}\cdot I(x_i,y_i)+w_{edge}\cdot\nabla I(x_i,y_i)\right) \tag{4}$$

where W_{line} and W_{edge} are adjustable constants controlling the contribution of each energy type.

Snake Evolution Equation

The contour varies its size and shape through the combination of the internal and external forces on each control point. By utilizing the forces defined in the previous section, the contour evolution from step $k-1$ to k can be defined as

$$\mathbf{x}_k=\mathbf{x}_{k-1}+\varepsilon\nabla\mathbf{E}(\mathbf{x}_{k-1}) \tag{5}$$

where ε is the step size, $x_k=(x_1, x_2, \cdots, x_L)_k^T$, $E(x_k)=(E_1, E_2, \cdots, E_L)$ and $E_i=E_{\text{int},i}+E_{\text{ext},i}$.

Unscented Kalman Filter

The Kalman filter has a structure consisting of the following processes. First, the estimation of the current state and the measurement are obtained by using the physical dynamics and the measurement model. Next, the Kalman gain which minimizes the estimation error is obtained by calculating the actual measurement. Finally, the gain is used to revise the estimated measurement to get a more accurate estimation of the current state. In the case of nonlinear dynamics, the Kalman filter can be extended as a nonlinear tracker by linearizing the nonlinearity within a certain measurement domain. This process is called the Extended Kalman Filter (EKF), and has been widely used because of its rapid processing time and satisfactory accuracy. EKF uses the first term of the Taylor expansion of the nonlinear dynamics equation. However, in the case of strong nonlinearity of dynamics and/or a large initial estimation error, this linearization of a nonlinear model may not guarantee stability (12). Therefore, the Unscented Kalman Filter (UKF) is designed to compensate for this linearization problem using the nonlinear model directly without linearizing it with specific points selected through the probabilistic distribution of estimated values (11).

Unlike EKF, UKF does not use the approximation of the nonlinear state-space model and exploits the nonlinear model directly. In UKF, the distribution of state is represented by using a Gaussian random variable. However, UKF denotes certain points called sigma points, which are obtained by using the mean and covariance of the distribution. The sigma points are used to proceed with time and measurement updates. By directly using the nonlinear model, UKF may overcome the problem of EKF resulting from linearization, regardless of high order terms in the Taylor expansion (12).

UKF uses an unscented transformation to solve the problem caused by the linearization process of EKF. UKF selects specific points based on the probabilistic distribution and applies them to directly the nonlinear model. This transformation is the core algorithm of UKF. Unscented transformation is a method for calculating the statistics of a random variable in nonlinear transformation and is based on the approximation of the distribution of the random variable (10).

Assume that a random variable x, ($L\times1$)is propagated using a nonlinear propagation function $f(\cdot)$ as $y=f(\mathrm{x})$. If the mean and covariance of the random variable x are given by $\bar{\mathrm{x}}$ and P_X, respectively, the $2L+1$ sigma points x_i and their weights W_i are decided as:

$$
\begin{aligned}
&\chi_0 = \bar{\mathbf{x}}, \quad i = 0,\\
&\chi_i = \bar{\mathbf{x}} + \left(\sqrt{(L+\kappa)\mathbf{P}_x}\right)_i, \quad i = 1,\cdots,L,\\
&\chi_i = \bar{\mathbf{x}} - \left(\sqrt{(L+\kappa)\mathbf{P}_x}\right)_i, \quad i = L+1,\cdots,2L,\\
&W_0 = \kappa/(L+\kappa), \quad \text{and}\\
&W_i = 1/\{2(L+\kappa)\}, \quad i = 1,\cdots,2L
\end{aligned}
\tag{6}
$$

where k is a scale parameter, W_i is the weight of the ith i^{th} sigma point and $\left(\sqrt{(L+\kappa)\mathbf{P}_x}\right)_i$ is the i^{th} column of the matrix square root. Based on the sigma points, it is possible to obtain the statistics of y. Each sigma point is propagated through the nonlinear function f as $\psi_i=f(x_i)$. Then, the estimated mean and covariance of the propagated sigma points becomes:

$$
\bar{\mathbf{y}} = \sum_{i=0}^{2L} W_i \Psi_i, \quad \mathbf{P}_y = \sum_{i=0}^{2L} W_i \left(\Psi_i - \bar{\mathbf{y}}\right)\left(\Psi_i - \bar{\mathbf{y}}\right)^T . \tag{7}
$$

The mean and the covariance calculated by using (7) have an accuracy up to the second term of the Taylor expansion for an arbitrary nonlinear function $f(x)$ compared to the first term in EKF (8). In addition, the amount of error can be adjusted by controlling the value of k.

In using the UKF, it is most important to determine sigma points in the unscented transformation. Nevertheless, it is noticeable that the probability of selecting sigma points in (6) deviated from the original mean and covariance is also increased as the dimension L of the state vector x is increased. This makes it difficult to maintain the original state distribution. In particular, in the case of high nonlinear function, the probability increases. To overcome this problem, it is necessary to choose the value of κ very carefully so as to not be deviated from the distribution of original sigma points.

Unscented Kalman Snake for Vessel Tracking

State-Space Model

The alteration of the cross section of a blood vessel over the inter-slices can be separated into two parts. One is *global rigid motion* and the other is *shape deformation* changing over its cross-section (14). The global rigid motion can be thought of as a translation of the centroid, and the deformation can be explained by a deformation function as described by the snake. Therefore, we suggest a tracking method by taking advantage of UKF and the snake over the cross-section of a blood vessel between slices. To achieve this, we composed the state vector of the centroid of the vessel contour, x_m, (2×1), and the control

point vector of snake, x_c, ($2L\times1$). In other words, the state vector at time step t is composed of $x_t=(X_m^T, X_c^T)^T_t$. Meanwhile, the measurement vector y_t for the observation space model is composed of centroid y_m and control points y_c, namely $y_t=(Y_m^T, Y_c^T)^T_t$. The respective covariance matrices of a priori and a posteriori estimates are:

$$\mathbf{P}_{k+1}^{-} = diag(\mathbf{P},\Sigma), \quad \mathbf{R} = diag(\mathbf{R}_{\mathbf{X}},\mathbf{R}_{\Sigma}) . \tag{8}$$

where $\mathbf{P}$ and $\mathbf{P}^{yy}$ are the (2×2) covariance matrix for the centroid coordinate, and Σ and Σ^{yy} are the ($2L\times2L$) diagonal matrices. The process noise covariance matrix $\mathbf{Q}$ and the measurement noise covariance matrix $\mathbf{R}$ are assumed to be constants as:

$$\mathbf{Q} = diag(\mathbf{Q}_X, \mathbf{Q}_\Sigma), \text{ and } R=diag(R_X, R_\Sigma). \tag{9}$$

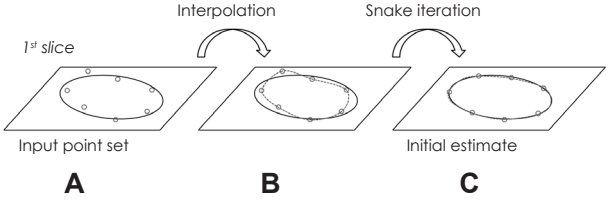

Fig. 3. Schematic diagram of the unscented Kalman snake for vessel tracking - Initialization (A) Input point set. (B) Interpolated input points. (C) After Snake iteration.

Measurement Model

At time step t, the nonlinear measurement function h accepts the seed point X_k whose dimension is $2M+2$ and the image I_k as an input. The function is composed as follows.

1) A closed contour h is created through the two-dimensional interpolation of M control points.

2) An evolved closed contour is obtained by using the snake iterations. The number of iterations can vary depending on the contour shape.

3) The evolved contour is re-sampled, and new control points are generated. Based on these points, a new centroid is also calculated.

The measurement function $h(X_k, I_k)$ has high nonlinearity because of snakes, which is the primary reason for using UKF instead of the classical Kalman filter.

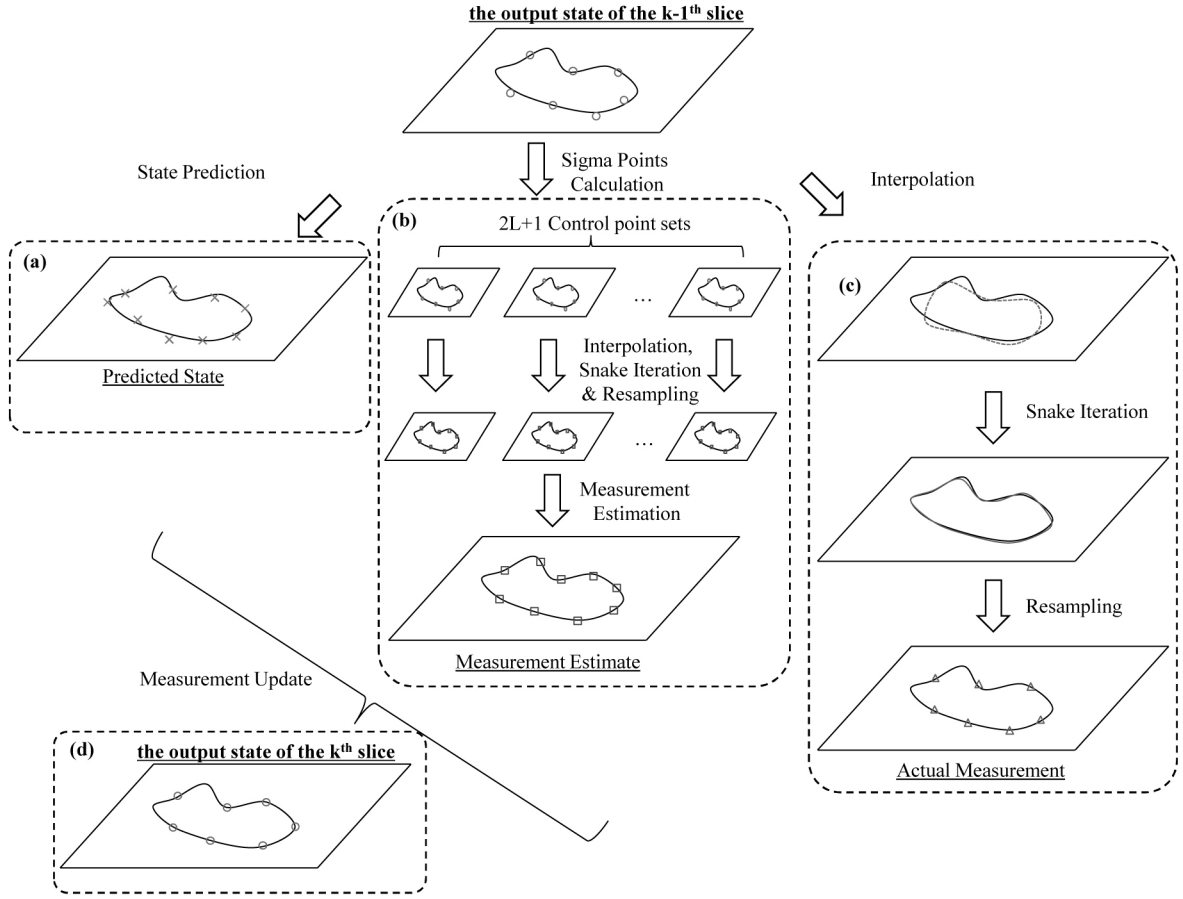

Fig. 4. Schematic diagram of the unscented Kalman snake for vessel tracking - Iteration (A) State prediction. (B) Snake iteration for sigma points. C: Measurement estimation. D: Measurement update.

Algorithm

Based on the aforementioned processes, the algorithm can be summarized as:

• Initialization - first slice

1) points around the vessel boundary for tracking are taken from the user in Fig. 3A.

2) L points are interpolated in Fig. 3B.

3) Interpolated points are accepted as input from the snake iterations, and an estimate of the vessel boundary is obtained for the first slice by the snake iterations in Fig. 3C.

• Iteration k^{th} slice

1) Based on the estimate of the k–1^{th} slice, state vectors are propagated by using the state-space model. The predicted state of the kth slice is obtained and depicted as point 'x' in Fig. 4A.

2) A control point set of $2L$+1 sigma points and their corresponding weights are generated by using the result from the estimate of the k–1^{th} slice. After this, each sigma point undergoes the three operations - interpolation, snake iteration, and resampling.

3) The estimate of the k–1^{th} slice is interpolated, and the result is processed by the snake iteration. This result is from the result for the estimate of the vessel boundary of the kth slice. Next, for the measurement update process for the Kalman filter, the state vector for the actual measurement is created through resampling. This process is shown in Fig. 4C.

4) Afterward, the covariance matrix and the Kalman gain are calculated. In addition, the estimated state vector for the kth slice is obtained by the measurement update process of the Kalman filter. This process is shown in Fig. 4D.

Results

We demonstrate the simulation results for the artery tracking applied using chest CT slices. The test slices are CTA images of a chest and are composed of 467 images having a 512× 512 resolution. The CTA images were obtained with a Discovery CT750 HD of General Electric Company. For the performance verification, the segmented results of a blood vessel were demonstrated over multiple CTA slices. To obtain the measurement prediction and the actual measurement, each process conducted 15 snake iterations.

To utilize the snake algorithm, the parameters for the internal and external energies in (3) and (4) need to be decided. The related parameters are α_i and β_i in (3) for the internal energy and w_{line} and w_{edge} in (4) for the external energy. To simplify the experiment, we use $\alpha=\alpha_i$ and $\beta=\beta_i$ for .

Internal Parameters

By varying the values of α and β, the shape variation of the contours are examined for the same user input and iteration number to determine the appropriate values of α and β for the simulation. The values of and vary from 0.1 to 2.0 as shown in Fig. 5, while the other parameters are fixed as w_{line} = 0.1, = w_{edge}0.1 for 20 iterations.

External Parameters

To determine w_{line} and w_{edge}, we examine the shape variation of contours w.r.t. those parameters, while α and β are fixed. In general, to find appropriate values of w_{line} and w_{edge}, α needs to be set at 0.1 because it gives the best performance, as shown in Fig. 5. However, when α=0.1, the vessel boundary is almost perfectly segmented, even if w_{line} and w_{edge} are arbitrarily selected in the range of 0 to 2.0. In such a case, it is difficult to find suitable values for w_{line} and w_{edge} because the vessel is segmented precisely, regardless of the values of and . However, when , the vessel is not segmented correctly, depending on the values of w_{line} and w_{edge}. Therefore, it is necessary to find w_{line} and w_{edge} when α is not optimally found. Here, we set α=0.5 for obtaining the segmentation while changing the values of w_{line} and w_{edge}.

Artery Tracking with Unscented Kalman Snake

Fig. 7 shows the results of vessel tracking on the chest CTA images by using the proposed algorithm. In Fig. 7A, the first measurement estimate is obtained in terms of brightness, edge information, shape, and size elasticity of the contour itself. The

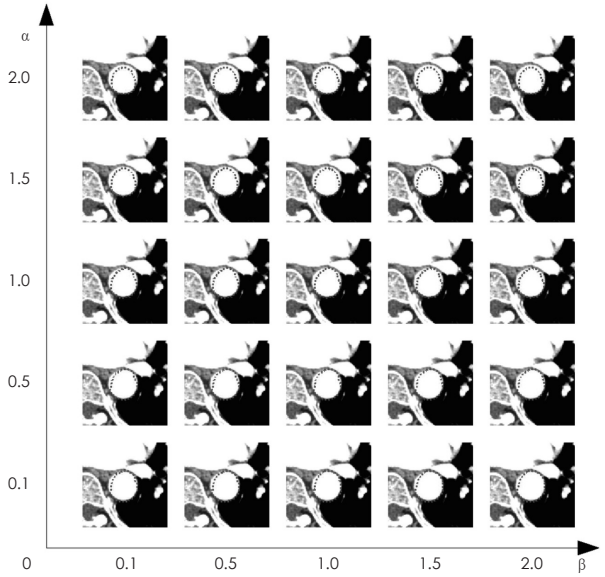

Fig. 5. Results of snake iteration for W_{line}=0.1 and W_{edge}=0.1 while varying α and β. For a given fixed α, there is a small variation in the contour w.r.t β, and for a given fixed β, the α more increases, the more the contour shrinks compared to its initial shape.

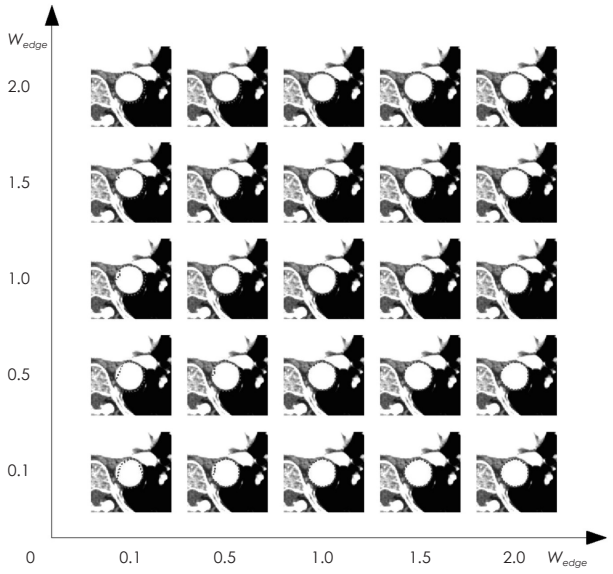

Fig. 6. Result of Snake iteration for α=0.1 and β=0. while varying W_{line} and W_{edge}. For a given W_{edge}, as the value W_{line} of increased, the contour over-segments the vessel boundary. In addition, for a given W_{line}, as the value of wedge is increased, the contour is close to the boundary of the vessel.

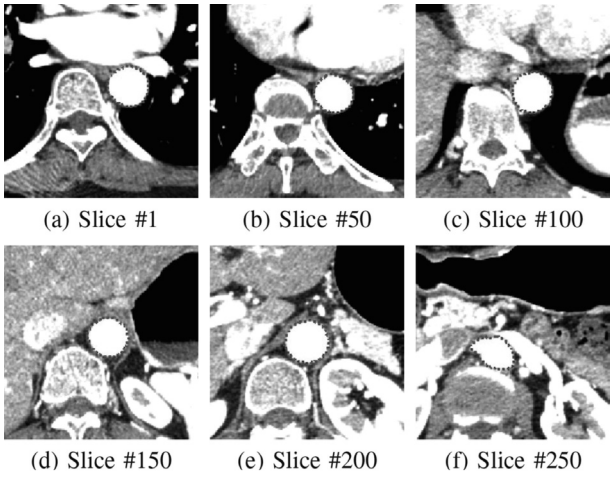

Fig. 7. Artery tracking example for every 50 frames. The red line shows the segmented vessel contour.

generated information effects the a posteriori information on the next CTA frame. For the following frames, the vessel is tracked through the more detailed tracking process utilizing Snake and UKF. As a result, the blood vessel can be tracked along with the artery, and the results for every 50 frames are shown in Fig. 7. For each slice, the segmented blood vessel is highlighted by the dotted line. As the slice propagates, it is shown that the position and shape of the blood vessel are deformed, and the proposed algorithm tracks the blood vessel accordingly.

3D Visualization of a Tracked Vessel

Fig. 8 represents the 3D visualization of the tracked artery

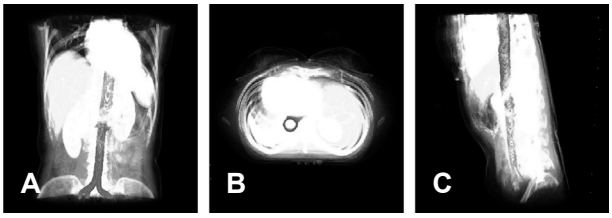

Fig. 8. 3D visualization of a segmented vessel. The tube-shaped middle line shows arteries.

based on the results from the previous section. For high speed 3D visualization, the graphics hardware (GeForce GTX 560Ti of NVIDIA) is exploited. According to Fig. 8, the segmented blood vessel is highlighted in red, and the other organs and bones are represented as a semitransparent color. The coronal, transverse and sagittal slices of the chest are represented in (A), (B), and (C), respectively, and the blood vessels for segmentation are classified properly.

Discussion

As stated in Section II, between snake iterations, the elasticity of the contour is increased as α is increased. It can be identified in Fig. 5, for a given fixed value of β, the more α increases, the more the contour shrinks compared to its initial shape. On the contrary, the shape variation w.r.t. β is slight because the initial snake iteration is operated on the bilinear interpolated control points of user input; meaning, as the interpolated shape using the initial points becomes round, it is still maintained through the iteration without changing its shape much. Thus, it can be stated that the contour is almost independent of β. Therefore, the contour will tightly adhere to the vessel boundary relying on the value of α.

Fig. 6 shows the results of snake iteration for α=0.5 and β=0.5 while varying w_{line} and w_{edge}. When is fixed, as the value of w_{line} is increased, the contour deforms its shape into the vessel boundary, especially when w_{edge} is low (i.e., in the range of 0.1 to 0.5), and the contour is extended outside of the boundary, meaning it is over-segmented. As mentioned in Section II, w_{line} is the parameter related to the pixel intensity, and the result shows that the greater is the weight w_{line} for the snake energy equation, the better the contour segments the boundary. Moreover, if w_{line} is fixed, the contour deforms and fits well on the boundary as w_{edge} is increased.

Conclusion

In this paper, we investigated a 3D vessel tracking algorithm called the unscented Kalman snake by jointly employing snake and the Kalman filter, both of which have been widely used for

automatic control algorithms in the area of computer vision. The arbitrarily shaped blood vessel boundary on each slice is segmented by using the active contour model, and a Kalman filter is employed to track the translation and shape deformation between CTA slices. The proposed algorithm is applied to the 3D visualization of chest CTA images using graphics hardware. Through this algorithm, more opportunities, giving quick and brief diagnosis, could be provided for the radiologist before detailed diagnosis using 2D CTA slices. Also, for the surgeon, the algorithm could be used for surgical planning, simulation, navigation and rehearsal, and is expected to be applied to highly valuable applications for more accurate 3D vessel tracking and rendering.

Acknowledgements

This work was supported by ETRI R&D Program [14ZC1400, The Development of a Realistic Surgery Rehearsal System based on Patient Specific Surgical Planning] funded by the Government of Korea.

REFERENCES

1. Bołdak C, Rolland Y, Toumoulin C, Coatrieux J. An improved model-based vessel tracking algorithm with application to computed tomography angiography. Journal of Biocybernetics and Biomedical Engineering 2003;3:41-64
2. Klein A, Egglin T, Pollak J, Lee F, Amini A. Identifying vascular features with orientation specific filters and b-spline snakes. In: Computers in Cardiology 1994: IEEE, 1994; 113-116
3. Klein AK, Lee F, Amini AA. Quantitative coronary angiography with deformable spline models. Medical Imaging, IEEE Transactions on 1997;16:468-482
4. Molina M, Prause GP, Radeva P, Sonka M. 3d catheter path reconstruction from biplane angiograms. In:Medical Imaging'98: International Society for Optics and Photonics, 1998;504-512
5. Chutatape O, Zheng L, Krishnan S. Retinal blood vessel detection and tracking by matched gaussian and kalman filters. In: Engineering in Medicine and Biology Society, 1998. Proceedings of the 20th Annual International Conference of the IEEE: IEEE, 1998;3144-3149
6. Yedidya T, Hartley R. Tracking of blood vessels in retinal images using kalman filter. In:Digital Image Computing: Techniques and Applications (DICTA), 2008: IEEE, 2008;52-58
7. Kass M, Witkin A, Terzopoulos D. Snakes: Active contour models. International journal of computer vision 1988;1:321-331
8. Julier SJ, Uhlmann JK, Durrant-Whyte HF. A new approach for filtering nonlinear systems. In:American Control Conference, Proceedings of the 1995: IEEE, 1995;1628-1632
9. Kalman RE. A new approach to linear filtering and prediction problems. Journal of Fluids Engineering 1960;82:35-45
10. Julier SJ, Uhlmann JK. New extension of the kalman filter to nonlinear systems. In:AeroSense'97: International Society for Optics and Photonics, 1997; 182-193
11. Lefebvre T, Bruyninckx H, De Schuller J. Comment on "a new method for the nonlinear transformation of means and covariances in filters and estimators"[with authors' reply]. Automatic Control, IEEE Transactions on 2002;47:1406-1409
12. Wan EA, Van Der Merwe R. The unscented kalman filter for nonlinear estimation. In:Adaptive Systems for Signal Processing, Communications, and Control Symposium 2000. AS-SPCC. The IEEE 2000: IEEE, 2000;153-158
13. Dougherty G. Digital image processing for medical applications: Cambridge University Press, 2009
14. Soatto S, Yezzi AJ. Deformotion deforming motion, shape average and the joint registration and segmentation of images. InComputer vision—eccv 2002: Springer, 2002:32-47